Pressure-induced excimer formation and fluorescence enhancement of an anthracene derivative†

Yuxiang Dai, ‡[ab] Haichao Liu,‡[c] Ting Geng,[d] Feng Ke,[be] Shanyuan Niu,[be] Kai Wang,[d] Yang Qi, *[af] Bo Zou, *[d] Bing Yang, *[c] Wendy L. Mao[be] and Yu Lin *[b]

Excimer materials have been widely studied and have generated significant interest for their applications in many optoelectronic devices. However, a thorough investigation of the entire process involved in excimer formation, enhancement, and annihilation in solid materials is still lacking. Here we designed a crystal based on an anthracene derivative with dissociative, molecular-ordered dimer assembly, and studied the formation and evolution of an anthracene excimer as a function of pressure. During the initial stage of pressurization, the fluorescence intensity arising from anthracene monomers gradually decreases. With continued compression, the two anthracene units become increasingly closer allowing strong intermolecular π–π interactions to develop that lead to excimer formation at 3.5 GPa, accompanied with a phase transition. The fluorescence intensity then keeps increasing with pressure and reaches its maximum at 5.6 GPa due to the strengthening of the excimer and the increased structural defects. Meanwhile the fluorescence color shows a continuous redshift, which initially results from conformation planarization and then excimer evolution. After releasing pressure back to ambient conditions, the structural changes in the sample are reversible, while the fluorescence signal preserves some high-pressure features due to the partial retention of the π–π interactions between the anthracene dimers. This study reveals the evolution of an excimer and its intrinsic photophysical properties, and provides guidance for future research on pressure-sensitive fluorescent devices.

Introduction

As a dimeric excited-state species, an excimer is formed by associating a ground-state molecule with a corresponding excited-state molecule. The fluorescence of an aromatic excimer was first reported by Förster and Kasper in a pyrene solution.[1] Subsequently, diverse types of aromatic excimers have been widely studied in solid-state materials especially in crystals.[2–10] Since excimers usually exhibit a red-shifted, structureless and broadened emission spectrum, relative to that of a monomer, they have found many applications in the fields of organic optoelectronic devices, organic lasers, chemical sensors and biological probes.[11–29]

Usually, a preformed dimer geometry in a ground state can be excited by light to readily form an excimer, so crystallographic methods are effective means to determine the dimer geometry. Among many intermolecular interactions, the π–π interaction is commonly observed in the above-mentioned dimer geometry. The formation and photophysical properties of an aromatic excimer are strongly dependent on the interplanar distance and the degree of overlap of the π–π dimer.[20–29] In general, a smaller interplanar distance and a greater overlapping area induce a larger red-shift of the emission spectrum of an excimer.[30] However, it is very difficult to track the evolution of the dimer geometry experimentally, which has hindered a deep understanding of excimers and their applications. Previous studies have suggested that supramolecular interactions such as π–π interactions can be efficiently modulated by external pressure, accompanied by changes in photophysical properties.[31–36] At high pressure, some organic fluorescent materials not only experience a wide range of fluorescence color changes,

[a] Department of Materials Physics and Chemistry, School of Materials Science and Engineering, Northeastern University, Shenyang, 110819, China
[b] Stanford Institute for Materials and Energy Sciences, SLAC National Accelerator Laboratory, Menlo Park, California 94025, USA. E-mail: lyforest@stanford.edu
[c] State Key Laboratory of Supramolecular Structure and Materials, College of Chemistry, Jilin University, Changchun 130012, China
[d] State Key Laboratory of Superhard Materials, College of Physics, Jilin University, Changchun 130012, China
[e] Department of Geological Sciences, Stanford University, California 94305, USA
[f] Key Laboratory for Anisotropy and Texture of Materials, Ministry of Education, Northeastern University, Shenyang 110819, China

† Electronic supplementary information (ESI) available. CCDC 2025392. For ESI and crystallographic data in CIF or other electronic format see DOI: 10.1039/d0tc04677a

‡ These authors contributed equally to this work.

but also show significant pressure-induced emission enhancement, which disobeys traditional aggregation-caused quenching (ACQ) theory. The enhancement arises from the inhibited nonradiative transitions due to the suppression of the vibration or the rotation of the molecules (*i.e.* the aggregation-induced emission (AIE) effect).[37–40] Moreover, the family of excimer materials that show emission enhancement has become one of the most promising candidates for potential luminescent applications.[41–43] In this work, we designed an anthracene derivative as a model system and combined optical and structural analysis to study the entire process of excimer formation, photoluminescence (PL) enhancement, and annihilation in a crystal in response to external pressure.

Results and discussion

Anthracene (**AN**) is a common luminophore for constructing an excimer.[44–49] In order to explore the formation mechanism of an excimer under high pressure, we designed 9-(5′-phenyl-[1,1′:3′,1″-terphenyl]-3-yl)anthracene (**PTA**) based on the unilateral **AN** molecule.[32] The aromatic substituents along one side of the **AN** plane act as spacers which isolate the two **AN** units (Fig. 1, left and Fig. S3, ESI†). At ambient conditions, **PTA** crystallizes in a monoclinic *C*2/*c* structure, and apparent physical stacking of **AN** dimers was observed within the crystal structure. However, the interplanar distance of 3.934 Å is larger than the typical distance (3.4–3.7 Å)[41,50] required to form the π–π stacking. There is no overlap between the two **AN** molecules from the top view. Moreover, the emission spectrum of the **PTA** crystal at ambient conditions (Fig. S4, ESI†) is very similar to that of the monomer (Fig. S6 and S7, ESI†). All these pieces of evidence support that the initial intermolecular interaction between the two **AN** planes, if existing, are very weak, and the emission characteristic of **PTA** is dominated by the individual **AN** unit.

High-pressure PL experiments were performed to investigate the evolution of the fluorescence behaviour in the pristine **PTA** crystal up to 12.0 GPa. The emission spectra of **PTA** were shown in Fig. 2(a) and Fig. S8(a–c) (ESI†). Upon initial compression to 1.0 GPa, the PL intensity shows continuous quenching, while preserving the entire vibrational structure that is assigned to the emission

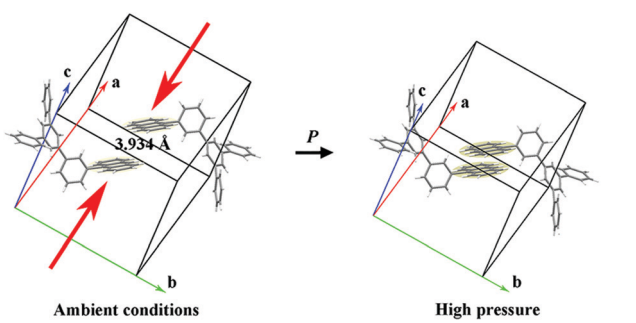

Fig. 1 Schematic of dimeric **PTA** molecules in the crystal at ambient conditions (left) that form an excimer at high pressure (right). Beige disks highlight the **AN** groups. The interplanar distance between the two adjacent **AN** planes is 3.934 Å at ambient conditions. The red arrows indicate the direction in which the adjacent **AN** planes approach.

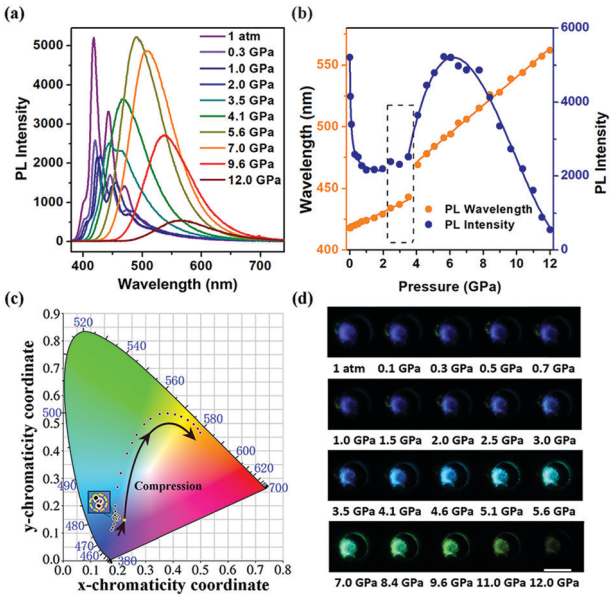

Fig. 2 (a) Representative emission spectra, (b) the evolution of the PL intensity and the emission wavelength, (c) pressure-dependent chromaticity coordinates of the emission (a magnified view of the yellow dashed circle area is shown inside the small square), and (d) fluorescence images of the **PTA** crystal from 1 atm to 12.0 GPa (the scale bar is 100 μm).

of an **AN** unit.[33] As pressure increases from 1.0 GPa to 3.5 GPa, the trend reverses and the PL intensity shows a gradual increase. The vibronic structures of the emission spectra start to disappear at about 3.5 GPa, and the emission is replaced by a broadened and structureless spectrum, which is the key characteristic of an excimer. As pressure continues to rise, the fluorescence intensity shows a steep increase up to 5.6 GPa beyond which it starts to decrease following the ACQ rule. So far, the previously reported excimer-induced emission enhancement has almost been exclusively based on the AIE effect.[41,51,52] In our case, an excimer was formed with subsequent pressure-induced emission enhancement, coinciding with a compression-induced transition to a high-pressure phase in which the structural defects increase with pressure, as we will discuss in a later section. Meanwhile PL spectra keep red-shifting from 418 nm to 562 nm as pressure increases from 1 atm to 12.0 GPa (Fig. 2b) due to molecular planarization[53] and excimer formation. It is worth noting that the wavelength shows an abrupt change when pressure exceeds 3.5 GPa, as marked by a dashed rectangle in Fig. 2b. This indicates that the broad PL peak starts to dominate the entire PL spectrum and a new dimer structure as of an excimer forms at about 4.0 GPa. Upon decompression, the PL intensity and color show a generally reversible trend, but a broad shoulder band in the long-wavelength region is retained in the emission spectrum of the released sample (Fig. S8(d), ESI†). This residual emission band can be ascribed to the intermolecular interactions between the **AN** units formed at high pressure being partially retained and then contributing to the recovered PL spectrum at ambient conditions.[33–35]

To investigate the excimer formation of **PTA** in aggregates, the emission spectra of **PTA** molecules in water-tetrahydrofuran

(THF) mixtures with varying water fraction (f_w) were collected (Fig. S9(a), ESI†). At f_w = 70% and above, **PTA** molecules start to aggregate, and a long-wavelength emission band gradually appears, which is similar to what we observed in the high-pressure experiment. This long-wavelength emission band has a long-lived component of 172.1 ns (Fig. S9(b), ESI†), in good agreement with the characteristics of a π–π **AN** excimer, *i.e.* a largely red-shifted and broadened emission spectrum with a long lifetime.[10] This supports that external pressure on the **PTA** crystal enables the **AN** excimer formation. Moreover, the varying emission spectra of the water–THF mixtures demonstrate no AIE effect for the **PTA** compound, because of the difference in the PL quantum yield of the crystalline sample and dilute THF solution which is 8% and 44%, respectively.

The pressure-dependent chromaticity coordinates were calculated to study how the emission changes (Fig. 2(c)). Below 0.3 GPa, the fluorescence color slowly redshifts. From 0.3 GPa to 2.5 GPa, the chromaticity coordinates fall in an extremely narrow region marked as the yellow dashed circle in Fig. 2(c). In particular, the chromaticity coordinates for pressures between 0.3 and 0.7 GPa nearly overlay on top of each other. This phenomenon is attributed to the conformational stability of the monomer without appreciable intermolecular interactions. When pressure reaches *circa* 3.0 GPa, the excimer starts to form that broadens the PL spectrum and eliminates the vibrational structure. The emission color of the evolving excimer continues to red-shift with increasing pressure likely as a result of the decreasing interplanar distance and/or widened overlap in excimer.[54] Upon decompression, the chromaticity results, the fluorescence images and stable emission spectra of the recovered samples (Fig. S10 and S11, ESI†) show that the PL wavelength has a semi-reversible trend where partial fluorescence color is retained at ambient conditions. Notably, all these color and intensity changes can be visually observed from the fluorescence images shown in Fig. 2(d) and Fig. S10(b) (ESI†).

In order to further verify the effect of molecular conformation and intermolecular interactions on the photophysical properties of **PTA** under high pressure, ultraviolet-visible (UV-Vis) absorption spectra were also collected (Fig. 3(a)). The absorption spectrum of the crystal at ambient conditions is similar to that of monomers in different solvents as shown in Fig. S12 (ESI†). Unlike the emission spectra which show drastic changes upon compression, absorption spectra exhibit continuous shifts with pressure. A direct-bandgap Tauc plot was used to determine the bandgap values (Fig. 3(b)). As pressure increases, the bandgap decreases at a rate of 53.3(7) meV GPa^{-1} from 1 atm to 11.9 GPa. The conformational planarization of monomers and the gradually enhanced π–π stacking cause this almost linear reduction of the bandgap.[1,28] This is because the ground-state geometry varies continuously with pressure. Upon decompression, the absorption spectra and the corresponding band gap values gradually revert back but do not completely return to their original state when pressure is fully released (Fig. S13, ESI†), which also indicates the intermolecular π–π interactions between the **AN** dimers are partially preserved.

To understand the relationship between the structure and PL changes in **PTA** at high pressure, synchrotron angle

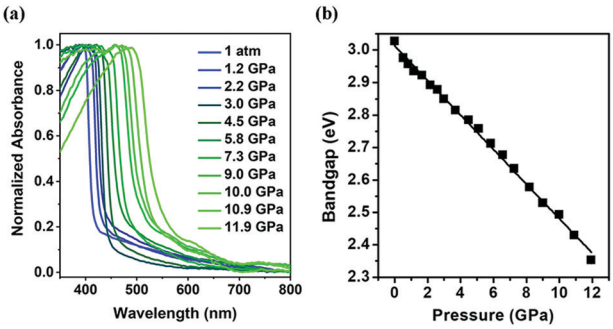

Fig. 3 (a) UV-Vis absorption spectra and (b) the calculated bandgap of the **PTA** crystal from 1 atm to 11.9 GPa. The uncertainty of the bandgap values is smaller than the symbol size.

dispersive X-ray diffraction (XRD) experiments were performed (Fig. 4(a)). The XRD pattern at 1 atm is in good agreement with the simulated one of the **PTA** crystal. With increasing pressure, all the XRD peaks shift to higher angles. As pressure reaches 3.5 GPa, a new reflection marked with an asterisk in Fig. 4(a) emerges, suggesting the onset of a phase transition. This peak grows in intensity as pressure increases. Furthermore, the peak profile around 2θ = 6.5 degree (marked by the dashed box in Fig. 4(a)) begins to change at 3.5 GPa; all the XRD peaks broaden which stems from the amorphous nature of the high-pressure phase up to 8.0 GPa, the highest pressure studied in the XRD measurements. The pressure at which the phase transition occurs followed by immediate amorphization coincides with that when the abrupt changes in the PL intensity and wavelength take place, as shown in Fig. 2(b), suggesting the formation of the dimer geometry of the excimer. Upon decompression, there was some hysteresis in the XRD patterns. After releasing pressure back to ambient conditions, the structural changes are fully reversible.

The evolution of the lattice constants up to 3.0 GPa is plotted in Fig. 4(b). The *a* and *c*-axes are more compressible than the

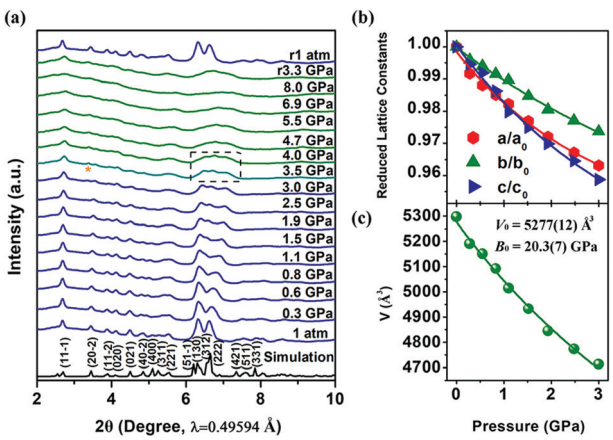

Fig. 4 (a) XRD patterns of **PTA** along compression from 1 atm to 8.0 GPa and decompression back to 1 atm. r represents releasing pressure. Lines in blue represent the initial phase, the cyan line represents the transitional state, and lines in green represent the high-pressure phase. (b) Evolution of the lattice constants and (c) unit cell volume as a function of pressure up to 3.0 GPa. Error bars are smaller than the symbol size.

b-axis, indicating the spacing along the π–π stacking as shown in Fig. 1 and Fig. S3 (ESI†) is compressed at a faster rate, and it is also obvious that **AN** molecules mainly slide along the *c*-axis. At the initial stage of pressurization, the rapid compression of the *a* and *c*-axes leads to the rapid approach between the **AN** groups, due to little intermolecular interactions between the monomers, as reflected in reducing the distance and increasing the slip degree. When pressure exceeds 1.0 GPa, the compression rate of the *c*-axis exceeds that of the *a*-axis, indicating that weak intermolecular interactions in the *a*-axis direction emerge, so that the approaching of the **AN** planes along the *a*-axis is gradually suppressed. A fitting of the experimental unit cell volume to a second-order Birch–Murnaghan equation of state yields a bulk modulus at ambient conditions of B_0 = 20.3(7) GPa (Fig. 4(c)), indicating the relatively loose molecular arrangement and compressible nature of the pristine crystal.

As pressure pushes the **AN** planes closer and closer along the *a*-axis, the weak interlayer interaction enhances the **AN** group sliding along the *c*-axis above 1.0 GPa. This weak interaction continues to strengthen from 1.0 GPa to 3.5 GPa, beyond which strong interactions, *i.e.*, π–π stacking interactions, likely form that induces excimer formation.[54] The continuous enhancement of intermolecular interactions likely triggers the phase transition, and the lowered energy difference between the excimer and the ground state causes the characteristic excimer peak to dominate the entire PL spectrum above 3.5 GPa. Albeit the increased rigidity of the **PTA** molecule, the reduced crystallinity of the material increases the defect concentrations, which mainly contributes to the further enhancement of the excimer emission band, according to previous reports.[33,55,56]

Raman spectroscopy measurements were performed to study the evolution of the molecular structure and arrangement of **PTA** under high pressure (Fig. S14, ESI†). From 1 atm to 10.5 GPa, all the external and internal modes show blue-shifts. Major Raman modes were assigned based on previous reports.[57,58] When pressure reaches 0.7 GPa, a new Raman external mode emerges (marked by an asterisk in Fig. S14(a), ESI†), which may indicate that weak intermolecular interactions start to change as close dimeric **AN** moieties are gradually forming. When pressure exceeds 4.4 GPa, all the Raman modes, especially the external modes, start to broaden, which suggest a reduction in the crystallinity. With further compression, the fluorescence background gradually increases and the signal-to-noise becomes worse. The frequency shifts of major internal Raman modes of **PTA** at selected pressures are plotted in Fig. S14(c) and (d) (ESI†). The linear trend indicates that the molecular structure is squeezed continuously. The regular blue-shifts of the CC stretching, CC bending and CH bending modes reflect gradual shrinkage of the phenyl rings. When pressure is released, the Raman spectrum recovers back to the initial state (Fig. S15, ESI†), consistent with the XRD results. In addition, these Raman results indicate that although the intermolecular interactions form when the excimer transition occurs, the molecular arrangement still resembles the starting phase and the molecular conformation changes gradually with compression.

Conclusions

In summary, we designed a system with initially discrete **AN** molecules (**PTA**), and monitored the photophysical evolution of the sample under high pressure. For the first time, we successfully followed excimer formation, strengthening and annihilation processes. From 1 atm to 12.0 GPa, the sample experiences a wide range of PL red-shifts (nearly 144 nm). Upon initial compression, the fluorescence intensity gradually decreases. At about 3.5 GPa, a transition to a high-pressure amorphous phase occurs and the excimer structure and π–π intermolecular interactions form. Further compression on the amorphous phase increases the structural defects that strengthen the excimer and lead to the enhancement of PL emission. Beyond 5.6 GPa, the PL intensity starts to decrease following the ACQ rule. The structural transition is reversible while the high-pressure optical properties are partially retained, when pressure is fully released. These results not only improve the understanding of excimer emission, but also provide guidance for designing new fluorescent materials.

Conflicts of interest

There are no conflicts to declare.

Acknowledgements

Work by Y. D. was supported by "the Fundamental Research Funds for the Central Universities" (No. N170203007 and N2002003), China Postdoctoral Science Foundation (No. 2018M631801), Postdoctoral Foundation of Northeastern University (No. 20180301) and financial support from the program of China Scholarships Council (No. 201906085035). Work by H. L. was supported by China Postdoctoral Science Foundation (No. 2018M641767) and Postdoctoral Innovation Talent Support Project (No. BX20180121). Work by F. K., S. N., W. L. M. and Y. L. was supported by the US Department of Energy (DOE) through the Stanford Institute for Materials and Energy Sciences DE-AC02-76SF00515. Work by K. W. was supported by National Natural Science Foundation of China (No. 11774120). Work by B. Z. was supported by National Natural Science Foundation of China (No. 21725304). Work by B. Y. was supported by National Natural Science Foundation of China (No. 91833304 and 51673083). XRD measurements were performed at beamline 12.2.2, Advanced Light Source, which is a US DOE Office of Science User Facility under contract no. DE-AC02-05CH11231.

Notes and references

1 T. Förster, *Angew. Chem., Int. Ed. Engl.*, 1969, **8**, 333.
2 J. B. Birks, *Rep. Prog. Phys.*, 1975, **38**, 903.
3 Y. Mizobe, M. Miyata, I. Hisaki, Y. Hasegawa and N. Tohnai, *Org. Lett.*, 2006, **8**, 4295.
4 Y. Mizobe, T. Hinoue, A. Yamamoto, I. Hisaki, M. Miyata, Y. Hasegawa and N. Tohnai, *Chem. – Eur. J.*, 2009, **15**, 8175.
5 J. Chen, A. Neels and K. M. Fromm, *Chem. Commun.*, 2010, **46**, 8282.

6 J. B. Birks, A. A. Kazzaz and S. F. Edwards, *Proc. R. Soc. London, Ser. A*, 1968, **304**, 291.
7 P. Coppens, S.-L. Zheng, M. Gembicky, M. Messerschmidt and P. M. Dominiak, *CrystEngComm*, 2006, **8**, 735.
8 P. E. Fielding and R. C. Jarnagin, *J. Chem. Phys.*, 1967, **47**, 247.
9 F. M. Winnik, *Chem. Rev.*, 1993, **93**, 587.
10 L. S. Kaanumalle, C. L. D. Gibb and B. C. Gibb, *J. Am. Chem. Soc.*, 2005, **127**, 3674.
11 Y. Liu, M. Nishiura, Y. Wang and Z. Hou, *J. Am. Chem. Soc.*, 2006, **128**, 5592.
12 B. W. D'Andrade and S. R. Forrest, *Adv. Mater.*, 2004, **16**, 1585.
13 J. Kalinowski, M. Cocchi, D. Virgili, V. Fattori and J. A. G. Williams, *Adv. Mater.*, 2007, **19**, 4000.
14 E. L. Williams, K. Haavisto, J. Li and G. E. Jabbour, *Adv. Mater.*, 2007, **19**, 197.
15 Y. Wang, J. Chen, Y. Chen, W. Li and C. Yu, *Anal. Chem.*, 2014, **86**, 4371.
16 J.-Y. Hu, Y.-J. Pu, F. Satoh, S. Kawata, H. Katagiri, H. Sasabe and J. Kido, *Adv. Funct. Mater.*, 2014, **24**, 2064.
17 L. Basabe-Desmonts, D. N. Reinhoudt and M. Crego-Calama, *Chem. Soc. Rev.*, 2007, **36**, 993.
18 H. Osaki, C.-M. Chou, M. Taki, K. Welke, D. Yokogawa, S. Irle, Y. Sato, T. Higashiyama, S. Saito, A. Fukazawa and S. Yamaguchi, *Angew. Chem., Int. Ed.*, 2016, **55**, 7131.
19 J.-Y. Hu, Y.-J. Pu, G. Nakata, S. Kawata, H. Sasabe and J. A. Kido, *Chem. Commun.*, 2012, **48**, 8434.
20 G. Mallesham, C. Swetha, S. Niveditha, M. E. Mohanty, N. J. Babu, A. Kumar, K. Bhanuprakash and V. J. Rao, *J. Mater. Chem. C*, 2015, **3**, 1208.
21 Y.-H. Chen, K.-C. Tang, Y.-T. Chen, J.-Y. Shen, Y.-S. Wu, S.-H. Liu, C.-S. Lee, C.-H. Chen, T.-Y. Lai, S.-H. Tung, R.-J. Jeng, W.-Y. Hung, M. Jiao, C.-C. Wu and P.-T. Chou, *Chem. Sci.*, 2016, **7**, 3556.
22 J. Lee, H. Jung, H. Shin, J. Kim, D. Yokoyama, H. Nishimura, A. Wakamiya and J. Park, *J. Mater. Chem. C*, 2016, **4**, 2784.
23 B. M. Chapin, P. Metola, S. L. Vankayala, H. L. Woodcock, T. J. Mooibroek, V. M. Lynch, J. D. Larkin and E. V. Anslyn, *J. Am. Chem. Soc.*, 2017, **139**, 5568.
24 R. Zhang, D. Tang, P. Lu, X. Yang, D. Liao, Y. Zhang, M. Zhang, C. Yu and V. W. W. Yam, *Org. Lett.*, 2009, **11**, 4302.
25 Y. Wang, J. Chen, H. Jiao, Y. Chen, W. Li, Q. Zhang and C. Yu, *Chem. – Eur. J.*, 2013, **19**, 12846.
26 G. Han, D. Kim, Y. Park, J. Bouffard and Y. Kim, *Angew. Chem., Int. Ed.*, 2015, **54**, 3912.
27 K. Nagarajan, S. K. Rajagopal and M. Hariharan, *CrystEng-Comm*, 2014, **16**, 8946.
28 S. Hisamatsu, H. Masu, M. Takahashi, K. Kishikawa and S. Kohmoto, *Cryst. Growth Des.*, 2015, **15**, 2291.
29 J.-Y. Hu, Y.-J. Pu, Y. Yamashita, F. Satoh, S. Kawata, H. Katagiri, H. Sasabe and J. Kido, *J. Mater. Chem. C*, 2013, **1**, 3871.
30 W. Jiang, Y. Shen, Y. Ge, C. Zhou, Y. Wen, H. Liu, H. Liu, S. Zhang, P. Lu and B. Yang, *J. Mater. Chem. C*, 2020, **8**, 3367.
31 H. Liu, Y. Dai, Y. Gao, H. Gao, L. Yao, S. Zhang, Z. Xie, K. Wang, B. Zou, B. Yang and Y. Ma, *Adv. Opt. Mater.*, 2018, **6**, 1800085.
32 H. Liu, Y. Gu, Y. Dai, K. Wang, S. Zhang, G. Chen, B. Zou and B. Yang, *J. Am. Chem. Soc.*, 2020, **142**, 1153.
33 Z. A. Dreger, H. Lucas and Y. M. Gupta, *J. Phys. Chem. B*, 2003, **107**, 9268.
34 H. W. Offen, *J. Chem. Phys.*, 1966, **44**, 699.
35 P. F. Jones and M. Nicol, *J. Chem. Phys.*, 1968, **48**, 5440.
36 P. F. Jones and M. Nicol, *J. Chem. Phys.*, 1965, **43**, 3759.
37 Y. Hong, J. W. Y. Lam and B. Z. Tang, *Chem. Soc. Rev.*, 2011, **40**, 5361.
38 J. Mei, N. L. Leung, R. T. Kwok, J. W. Lam and B. Z. Tang, *Chem. Rev.*, 2015, **115**, 11718.
39 Y. Hong, J. W. Y. Lam and B. Z. Tang, *Chem. Commun.*, 2009, 4332.
40 J. Mei, Y. Hong, J. W. Y. Lam, A. Qin, Y. Tang and B. Z. Tang, *Adv. Mater.*, 2014, **26**, 5429.
41 Z. Zhao, S. Chen, J. W. Y. Lam, Z. Wang, P. Lu, F. Mahtab, H. H. Y. Sung, I. D. Williams, Y. Ma, H. S. Kwok and B. Z. Tang, *J. Mater. Chem.*, 2011, **21**, 7210.
42 Y. Liu, X. Tao, F. Wang, J. Shi, J. Sun, W. Yu, Y. Ren, D. Zou and M. Jiang, *J. Phys. Chem. C*, 2007, **111**, 6544.
43 Y. Liu, X. Tao, F. Wang, X. Dang, D. Zou, Y. Ren and M. Jiang, *J. Phys. Chem. C*, 2008, **112**, 3975.
44 R. Martínez-Máñez and F. Sancenón, *Chem. Rev.*, 2003, **103**, 4419.
45 T. Hinoue, Y. Shigenoi, M. Sugino, Y. Mizobe, I. Hisaki, M. Miyata and N. Tohnai, *Chem. – Eur. J.*, 2012, **18**, 4634.
46 M. Sugino, Y. Araki, K. Hatanaka, I. Hisaki, M. Miyata and N. Tohnai, *Cryst. Growth Des.*, 2013, **13**, 4986.
47 R. Akatsuka, A. Momotake, Y. Shinohara, Y. Kanna, T. Sato, M. Moriyama, K. Takahashi, Y. Nishimura and T. Arai, *J. Photochem. Photobiol., A*, 2011, **223**, 1.
48 P. K. Lekha and E. Prasad, *Chem. – Eur. J.*, 2010, **16**, 3699.
49 G. Zhang, G. Yang, S. Wang, Q. Chen and J. S. Ma, *Chem. – Eur. J.*, 2007, **13**, 3630.
50 K. Nagura, S. Saito, H. Yusa, H. Yamawaki, H. Fujihisa, H. Sato, Y. Shimoikeda and S. Yamaguchi, *J. Am. Chem. Soc.*, 2013, **135**, 10322.
51 H. Liu, L. Yao, B. Li, X. Chen, Y. Gao, S. Zhang, W. Li, P. Lu, B. Yang and Y. Ma, *Chem. Commun.*, 2016, **52**, 7356.
52 Y. Shen, H. Liu, S. Zhang, Y. Gao, B. Li, Y. Yan, Y. Hu, L. Zhao and B. Yang, *J. Mater. Chem. C*, 2017, **5**, 10061.
53 Y. Zhang, Q. Song, K. Wang, W. Mao, F. Cao, J. Sun, L. Zhan, Y. Lv, Y. Ma, B. Zou and C. Zhang, *J. Mater. Chem. C*, 2015, **3**, 3049.
54 Y. Ge, Y. Wen, H. Liu, T. Lu, Y. Yu, X. Zhang, B. Li, S.-T. Zhang, W. Li and B. Yang, *J. Mater. Chem. C*, 2020, **8**, 11830.
55 M. Citroni, B. Costantini, R. Bini and V. Schettino, *J. Phys. Chem. B*, 2009, **113**, 13526.
56 S. Fanetti, M. Citroni and R. Bini, *J. Phys. Chem. B*, 2011, **115**, 12051.
57 N. Abasbegović, N. Vukotić and L. Colombo, *J. Chem. Phys.*, 1964, **41**, 2575.
58 J. Räsänen, F. Stenman and E. Penttinen, *Spectrochim. Acta*, 1973, **29**, 395.